Title

Optimizing the monomer structure of polyhedral oligomeric silsesquioxane for ion transport in hybrid organic–inorganic block copolymers

Journal

Journal of Polymer Science, 58(2)

ISSN

2642-4150

Authors

Gao, KW
Jiang, X
Hoffman, ZJ
et al.

Publication Date

2020-01-15

DOI

10.1002/pol.20190073

Peer reviewed

Optimizing the Monomer Structure of Polyhedral Oligomeric Silsesquioxane (POSS) for Ion Transport in Hybrid Organic-Inorganic Block Copolymers

Kevin W. Gao,[a,b,d] Xi Jiang,[b] Zach J. Hoffman,[a,b,d] Gurmukh K. Sethi,[b,c] Saheli Chakraborty,[a,b] Irune Villaluenga,[a,*] Nitash P. Balsara[a,b,d,*]

[a] *Department of Chemical and Biomolecular Engineering, University of California, Berkeley, California 94720, USA*

[b] *Materials Sciences Division, Lawrence Berkeley National Laboratory, Berkeley, California 94720, USA*

[c] *Department of Materials Science and Engineering, University of California, Berkeley, California 94720, USA*

[d] *Joint Center for Energy Storage Research (JCESR), Lawrence Berkeley National Laboratory, Berkeley, California 94720, USA*

* Correspondence to nbalsara@berkeley.edu and irvillaleunga@gmail.com

ABSTRACT

Poly(ethylene oxide)-*b*-polyhedral oligomeric silsesquioxane (PEO-POSS) mixed with lithium bis(trifluoromethanesulfonyl)imide salt is a nanostructured hybrid organic-inorganic block copolymer electrolyte that may enable lithium metal batteries. The synthesis and characteristics of three PEO-POSS block copolymer electrolytes which only differ by their POSS silica cage substituents (ethyl, isobutyl, isooctyl) is reported. Changing the POSS monomer structure results in differences in both thermodynamics and ion transport. All three neat polymers exhibit lamellar morphologies. Adding salt results in the formation of a disordered window which closes and gives way to lamellae at higher salt concentrations. The width of disordered window decreases with increasing length of the POSS alkyl chain substituent from ethyl to isobutyl and is absent in the isooctyl sample. Rheological measurements demonstrate good mechanical rigidity when compared with similar all-organic block copolymers. While salt diffusion coefficient and current ratio are unaffected by substituent length, ionic conductivity increases as the length of the alkyl chain substituent decreases: the ethyl substituent is optimal for ion transport. This is surprising because conventional wisdom suggests that ion transport occurs primarily in the PEO-rich domains, i.e. ion transport should be unaffected by substituent length after accounting for the minor change in conducting phase volume fraction.

INTRODUCTION

Solid polymer electrolytes are of interest for developing safer lithium batteries as they are less flammable than more traditional organic liquid electrolytes.[1–3] They may also enable the development of higher energy density batteries with lithium metal anodes.[4–5] In order to be used in lithium metal batteries, polymer electrolytes must have good ion transport properties as well as high mechanical rigidity to prevent lithium dendrite growth.[6] These two properties are decoupled in block copolymers such as polystyrene-*b*-poly(ethylene oxide) (SEO) wherein the polystyrene-rich microphase provides mechanical strength and the poly(ethylene oxide)-rich microphase enables ion transport when a salt such as lithium bis(trifluoromethanesulfonyl)imide (LiTFSI) is mixed with the copolymer.[7] The phase behavior of these materials is also important, as ion transport parameters such as ionic conductivity and salt diffusion coefficient are affected by morphology.[8] Most of the work in this area is restricted to all-organic block copolymer systems.[8–22]

Recent work has shown that hybrid organic-inorganic poly(ethylene oxide)-*b*-polyhedral oligomeric silsesquioxane (PEO-POSS) block copolymers with LiTFSI

self-assemble into a variety of morphologies with high mechanical rigidity and ionic conductivity when compared with SEO electrolytes of comparable molecular weight.[23] Like in SEO, the PEO-rich microphase facilitates ion transport via segmental motion,[24] while the POSS-rich microphase furnishes mechanical rigidity.[25] While it is clear that the thermodynamic interactions between PEO and POSS chains depend on the chemical structure of the silica cage substituents on the POSS monomer, effect of the cage structure on ion transport is an open question. While the impact of cage substituents on the thermal and morphological characteristics of nanocomposite polymer – POSS blends has often been studied,[26-35] sparse work on its effect upon phase behavior and ion transport in block copolymers exists.[36-38]

In this paper, we report on the synthesis of PEO-POSS block copolymers from three different POSS containing monomers (methacrylethyl, methacrylisobutyl, methacrylisooctyl POSS) whose cage substituents systematically increase in alkyl chain length. We use small angle X-ray scattering (SAXS) and transmission electron microscopy (TEM) to determine the morphology of these systems with and without added salt. The mechanical properties of the neat polymers are determined through rheological measurements. Finally, electrochemical characterization is used to study ion transport.

Conventional wisdom suggests that the chemical composition of the non-conducting microphase does not affect ion transport of block copolymer electrolytes, after effects related to changes in the morphology and volume fraction of the conducting phase are accounted for.[8,14,19.39-40] The purpose of this paper is to challenge this conventional wisdom.

EXPERIMENTAL

The PEO-POSS copolymers were synthesized, purified, and characterized using methods described in **ref 23** and reported in the Supporting Information (**Figures S1–S7**). The polymers used in this study are called PEO-POSS(5-1) where the 5 denotes the molecular weight of PEO in kg mol^{-1} and there is 1 POSS unit of varying molecular weight from 0.7 to 1.3 kg mol^{-1} due to the different alkyl chain substituent (ethyl, isobutyl, isooctyl) on the POSS silica cage. The chemical structure is shown in **Figure 1**.

We add LiTFSI salt to make electrolytes of varying salt concentration *r*, where we define *r* to be the molar ratio of lithium to ethylene oxide moieties. Electrolytes were prepared with methods described in **ref 23**. A list of the polymer characteristics can be found in **Table 1**. The neat copolymers are colorless.

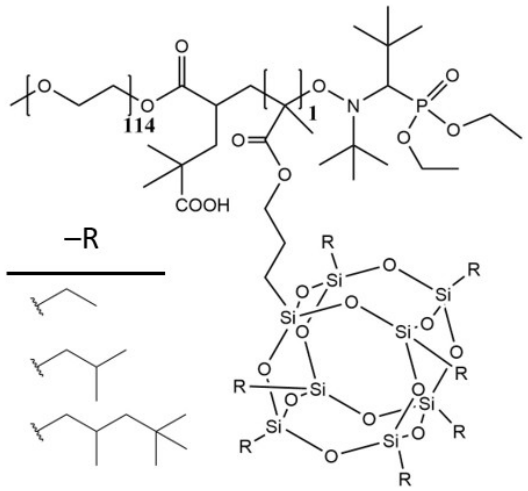

Figure 1. Chemical structure of PEO-POSS polymers synthesized. The alkyl substituent on the POSS silica cage increases in length from ethyl to isobutyl to isooctyl.

Table 1. Summary of PEO-POSS(5-1) characteristics

–R	M_{POSS} **(kg/mol)**	M_{PEO} **(kg/mol)**	$f_{EO/LiTFSI}$	***N***
Ethyl	0.7	5	0.87 – 0.93	85
Isobutyl	0.9	5	0.85 – 0.92	87
Isooctyl	1.3	5	0.79 – 0.88	95

Small angle X-ray scattering (SAXS)

SAXS samples were prepared by melt pressing the polymer into a 0.766 cm thick rubber spacers with a 0.3175 cm inner diameter, and annealing them at 90 °C for 3 hours, then 70 °C for 48 hours before allowing them to cool slowly under vacuum to room temperature. The samples were sealed with Kapton windows in custom-designed airtight aluminum holders.

SAXS measurements were performed at beamline 1–5 at the Stanford Synchrotron Radiation Lightsource and SLAC National Accelerator Laboratory and beamline 7.3.3 at the Advanced Light Source at Lawrence Berkeley National Laboratory.[41] Silver behenate was used to determine the beam center and sample-to-detector distance. The scattered intensity was corrected for beam transmission and empty cell scattering. Two dimensional scattering patterns were integrated azimuthally using the Nika program for IGOR Pro to produce one-dimensional scattering profiles and are reported as scattering intensity, I, as a function of the magnitude of the scattering vector, q.[42] Absolute scattering intensity, I_{abs}, was obtained by calibrating to a glassy carbon absolute intensity standard and is reported in the Supporting Information (**Figure S12**). Measurements were taken in a custom-built 8-sample heating stage at 70 °C, 90 °C, and 110 °C. Samples were equilibrated for about 20 min at each temperature before taking measurements. To a good approximation, the SAXS profiles of all our samples were independent of temperature in the temperature range of 70 – 110 °C and were similar upon heating and cooling. We only discuss data obtained at 70 °C in the main text in consistency with our electrochemical measurements.

The temperature range of our SAXS experiments is above the melting temperature of the semi-crystalline PEO block.

Electrochemical measurements

All sample preparation was performed inside of an argon glovebox with water and oxygen levels below 1 ppm and 2 ppm respectively. Conductivity cells were prepared by pressing the polymer electrolyte into a 254 μm thick silicone spacer with a 1/8 in. inner diameter and sandwiching between two 200 μm thick stainless-steel shim blocking electrodes. Lithium symmetric cells were prepared by pressing the polymer electrolyte into a 254 μm thick silicone spacer with a 1/8 in. inner diameter and sandwiching between two 180 μm thick lithium foils backed with stainless-steel shims. For both conductivity and lithium symmetric cells, nickel tabs were secured to the stainless-steel shims to serve as electrical contacts, and the assembly was vacuum sealed in laminated aluminum pouch material. Each cell was then taken out of the glovebox, placed in a custom-built heating stage, and annealed at 90 °C for 3 hours prior to electrochemical characterization. At the conclusion of the experiments, samples were taken back into the glovebox to check for defects and the assembly was measured to find the final sample thickness.

Complex impedance measurements were performed on the conductivity cells via a Bio-Logic VMP3 potentiostat over a 0.1 – 10^6 Hz frequency range at an amplitude of 80 mV to find the ionic conductivity, κ. Representative Nyquist plots are shown in the Supporting Information (**Figure S13**). Lithium symmetric cells were first conditioned for at least 4 charge/discharge cycles at a low current density of 0.02 mA cm^{-2} to ensure a stable interfacial layer was introduced. Each conditioning cycle consisted of a 4 h charge followed by a 2 h rest and a 4 h discharge. The Bruce and Vincent method was then used to find the current fraction, ρ_+, defined as

$$\rho_{+} = \frac{i_{ss}\left(\Delta V - i_{\Omega} R_{i,0}\right)}{i_{\Omega}\, R_{i,ss}}$$

where $R_{i,0}$ is the initial interfacial resistance, $R_{i,ss}$ is the interfacial resistance at steady-state, i_{ss} is the current measured at steady state, ΔV is the applied potential, i_Ω is a measure of the initial current, as defined by the ratio of the applied potential to the sum of the initial bulk and interfacial resistances.[43] The restricted diffusion method was used to find the salt diffusion coefficient, D.[44] Cells were polarized at +/- 10 mV and +/- 20 mV until a steady-state current was reached, then allowed to relax under open circuit potentials. Impedance was taken before and after polarization. Measurements were done at 70 °C.

In the literature, the parameter we call ρ_+ is often referred to as the transference number.[45] In our group, we have referred to it as the steady state cationic transference number, $t_{+,ss}$.

It has been shown that ρ_+ (or $t_{+,ss}$) is equal to the transference number in dilute and ideal electrolytes.[46] However, in concentrated electrolytes, and especially in concentrated polymer electrolytes, there is a significant difference in both magnitude and sign between ρ_+ and the transference number.[45-47] Since we are mainly interested in concentrated electrolytes in this work and it has been shown that PEO-containing electrolytes are highly non-ideal[47], we use the term ρ_+ to indicate the results of these experiments using the Bruce and Vincent method.

Rheology

The viscoelastic properties of the neat polymers were studied using the procedure outlined in **ref 48**, though samples were prepared by annealing at 70 °C instead of 120 °C. Measurements were repeated multiple times.–

Transmission electron microscopy imaging

The quenched PEO-POSS bulk samples were sectioned at -120 °C using a cryo-microtome (Leica Ultracut 6) to obtained ultrathin films (~100 nm). The ultrathin films were transferred to copper grids with lacey carbon supporting film and stored in an argon glovebox immediately after cryo-microtoming to minimize the effect of humidity. PEO-rich domains were stained to increase contrast and stability under the electron beam by exposing the ultrathin film to ruthenium tetroxide vapor for 10 minutes at room temperature. TEM micrographs were collected using Philips CM200 equipped with Gatan US1000 CCD camera.

RESULTS AND DISCUSSION

We performed SAXS experiments to elucidate the morphology of our electrolytes. Typical data obtained are shown in Figure 2 where scattering intensity measured at 70 °C is plotted as a function of the magnitude of the scattering vector. In **Figure 2a**, we show data obtained from ethyl samples with varying salt concentration. In the neat state, the ethyl polymer exhibits a lamellar morphology, as evidenced by the scattering peaks at $q = q^*$, $2q^*$, and $3q^*$ where q^* indicates the location of the primary scattering peak. Upon salt addition, at $r = 0.02$, the peaks diminish in intensity, and at $r = 0.06$ the peaks vanish, indicating the formation of a disordered phase. Upon further increase in salt concentration to $r = 0.12$, weak scattering peaks corresponding to a lamellar phase appear and their intensity increases with increasing salt concentration. In **Figure 2b**, we show data obtained from isobutyl samples with varying salt concentration. This polymer also forms a lamellar phase in the neat state. Increasing r to 0.02 results in a loss of the peak at $q = 2q^*$ and a significant reduction in scattering intensity at $q = q^*$. We attribute this weak scattering peak to the presence of disordered concentration fluctuations.[49] The isooctyl sample is lamellar in the

neat state with relatively sharp peaks at q^* and $2q^*$, as can be seen in **Figure 2c**. The addition of salt results in an increase in the scattering intensity at q values below q^* (in the range 0.20 $nm^{-1} \leq q \leq$ 0.35 nm^{-1}). At r = 0.08, a distinct shoulder is apparent in this q range. This shoulder becomes more pronounced with increasing salt concentration. At r = 0.3, we obtain broad scattering peaks that are reminiscent of the scattering peaks seen in the ordered ethyl and isobutyl samples.

To better quantify the ordering in our systems, we analyze the absolute scattering intensities of each sample. These profiles, qualitatively similar to the raw scattering profiles of **Figure 2**, are given in **Figure S12** in the Supporting Information. In **Figure 3a**, we show scattering in the vicinity of the primary peak for the ethyl sample at r = 0.02. A Lorentzian fit (with a linear background) through the data is shown by the curve. The primary peak after background subtraction is shown as a dashed curve in **Figure 3a**. This enables determination of the full-width-half-max (FWHM), which for the sample in **Figure 3a** is 0.082 nm^{-1}. In **Figure 3b**, we shown scattering in the vicinity of the primary peak for the isooctyl sample at r = 0.12. Clearly, a single Lorentzian is not consistent with this data set, and we thus use a two Lorentzian fit to characterize this sample. This enables determination of two FWHM values corresponding to the two peaks shown in **Figure 3b** (0.14 and 0.036 nm^{-1}). All of the scattering curves from the ethyl and isobutyl samples were analyzed using the approach

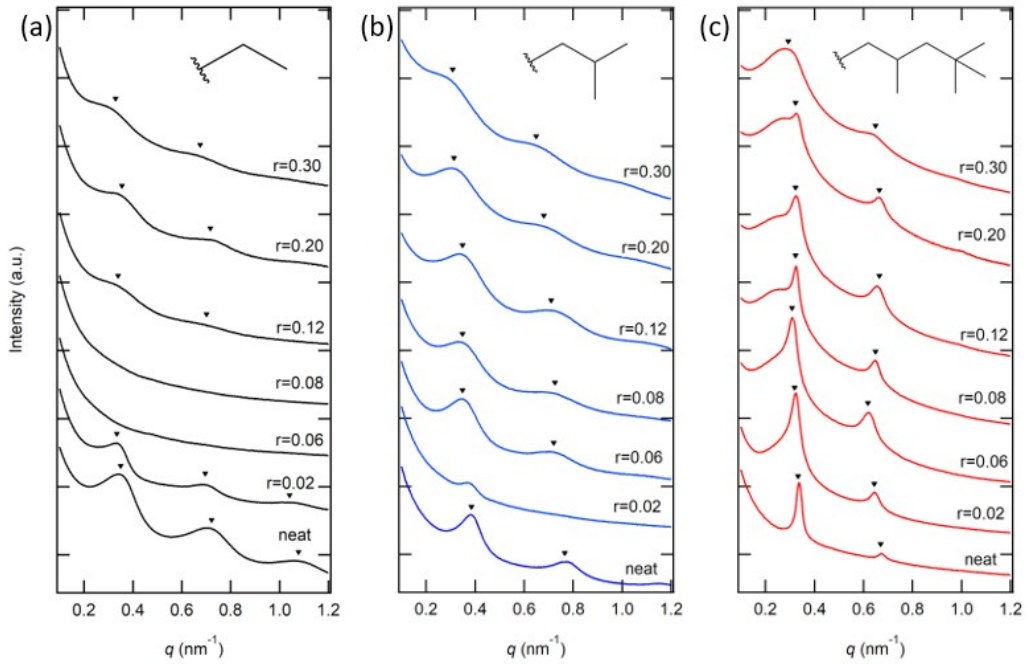

344**Figure 2.** Scattering intensity at 70 °C of the three PEO-POSS polymers with
345various salt concentrations, plotted as a function of the magnitude of the scattering
346vector, *q,* (a) ethyl (b) isobutyl and (c) isooctyl. Profiles are shifted vertically.
347Triangles indicate peaks at *q**, 2*q**, and 3*q** (when identified). These peaks signify
348lamellar order.

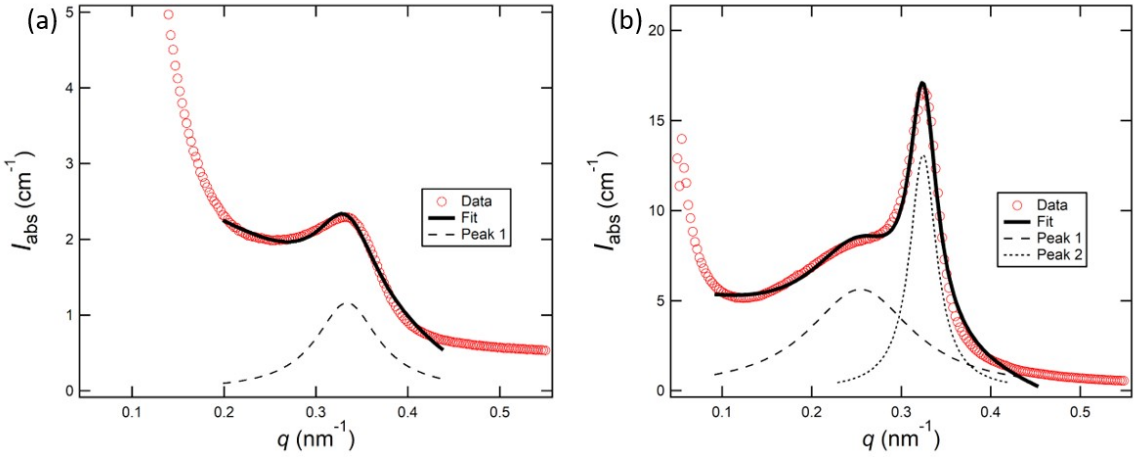

349 **Figure 3.** Lorentzian fits of the scattering around the primary peak for the (a) r =
350 0.02 ethyl sample, with a FWHM of 0.082 nm^{-1}, and the (b) r = 0.12 isooctyl sample,
351 which has FWHMs of 0.14 and 0.036 nm^{-1}.

352shown in **Figure 3a**. The scattering
353curve from the neat isooctyl
354sample was analyzed using one
355Lorentzian while the salty samples
356were analyzed using two
357Lorentzians as in **Figure 3b**.

358 In **Figure 4a** we compare
359the locations of the scattering

peaks in the salty isooctyl samples. There is a clear distinction between the broad and sharp peaks. In **Figure 4b**, we plot the FWHMs obtained from our fitting procedure outlined above. The widths of the primary scattering peaks

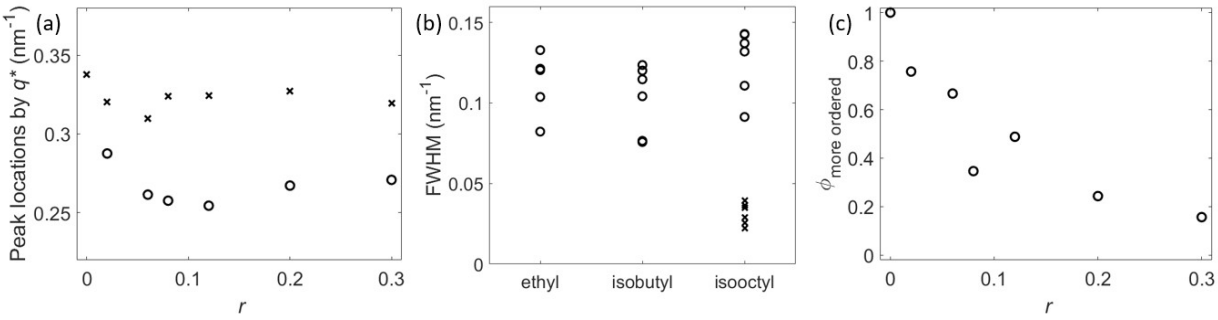

Figure 4. (a) Plot of the peak locations around q^* in the isooctyl samples versus salt concentration, where the circles denote the broad peaks and the x's denote the sharp peaks. (b) Plot of the full-width-half-max of the primary scattering peak versus POSS silica cage alkyl substituent, where circles denote the broad peaks found in the ethyl, isobutyl and salty isooctyl samples, and x's denote the sharp peaks in the isooctyl samples. (c) Plot of the volume fraction of the phase in the isooctyl electrolytes with more long range order versus salt concentration, r.

of the ethyl and isobutyl samples are similar, and we obtain FWHMs between 0.07 and 0.13 nm^{-1}. We obtain two sets of FWHM values for the isooctyl samples, one set that is qualitatively similar to that of the ethyl and isobutyl samples, and another with significantly lower FWHM values ranging from 0.02 to 0.04 nm^{-1}. It is perhaps interesting to note that the FWHM of the ordered phase formed in the neat isooctyl sample is qualitatively different than those obtained in the other samples, both with and without salt. The addition of salt to the isooctyl sample results in the emergence of a broad scattering profile that is qualitatively similar to that obtained from the other samples. The FWHM is generally assumed to be an indication of the extent of long range order. We conclude that the salt-containing isooctyl samples comprise two kinds of ordered phases with distinct extents of long range order. In **Figure 4c** we compare the volume fractions of the two coexisting phases in our salty isooctyl samples by integrating $I_{abs}q^2$ of the broad and sharp peaks (see **Figure 3b**) using a procedure outlined in **ref 50**. The volume fraction of the phase with greater long range order decreases with increasing salt concentration.

Samples were annealed at 70 °C and quenched in liquid nitrogen to "freeze" the morphology at these temperatures before performing electron microscopy. The resulting TEM micrographs are shown in **Figure 5**, where the dark phase represents the RuO_4 stained PEO-rich microphases. The micrographs obtained from those

samples show similar alternating dark and bright stripes, PEO-rich and POSS-rich domains, representing the lamellar phase separation. **Figure 5a** shows the typical lamellar morphology in the neat ethyl sample. As shown in **Figure 5b**, the lamellar structure in the isooctyl sample exhibits a more long-range ordered structure with larger spacing (*d*). In addition, the Fourier transforms of the micrographs suggest that the isooctyl sample has the largest *d* as compared to the *d* in neat ethyl sample and the salty isooctyl sample (r = 0.12). The distinction between the two kinds of lamellar phases in salty isooctyl samples is not evident by the micrograph in **Figure 5c**. We note that similar data (i.e. the presence of an additional peak in the vicinity of the primary peak) have been obtained from other salty block copolymers. The presence of coexisting phases is clearly seen by TEM in some cases[22-23], but not in others[51]. In **ref 51**, the presence of an

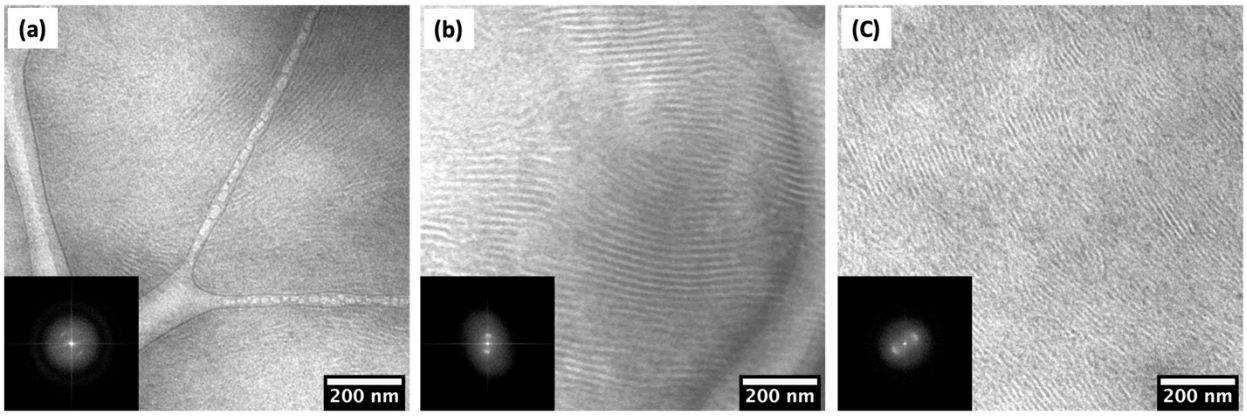

Figure 5. TEM micrographs of (a) neat ethyl sample, (b) neat isooctyl sample, and (c) isooctyl r = 0.12. The dark phase represents the RuO_4 stained PEO domain. Insets show the Fourier transforms of the micrographs. Lamellar order is seen in all cases.

additional peak was attributed to the formation of a superlattice. Further work is needed to establish the origin of the SAXS pattern shown in **Figure 4b**.

The effect of added salt and monomer structure on morphology is summarized in **Figure 6**. In ethyl and isobutyl samples, we only see lamellae and disorder. In the isooctyl samples, we see lamellae in the neat state and coexisting phases in the presence of added salt. The thermodynamic interactions between the PEO and POSS blocks in the presence of salt is complex. Disordered phases are formed upon salt addition but this applies to a limited window of salt concentrations. When this window is exceeded, ordered phases

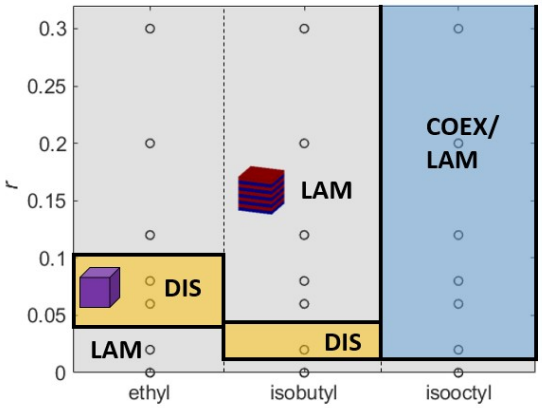

reappear at high salt concentrations. The salt concentration window for which disordering occurs decreases as we increase the POSS alkyl substituent chain length and is absent in the isooctyl sample. There are many possible reasons for the complex phase behavior seen in **Figure 6**. This includes differences in polarity of the POSS block, shielding of repulsive interactions between the POSS particle and PEO due to the presence of alkyl substituents, and the distribution of ions in PEO-rich and POSS-rich domains. Partial solubility of LiTFSI in the POSS-rich domains may account for differences in phase behavior. It is evident that segregation and phase separation in PEO-POSS(5-1) block copolymers is greatly affected by the functional groups on the POSS monomer.

Figure 6. Morphology of phases on a salt concentration, *r*, versus POSS silica cage alkyl substituent plot: lamellar (LAM) and disordered (DIS), as well as a coexistence of ordered phases (COEX/LAM).

We measured the ionic conductivity, salt diffusion coefficient, and the current ratio of the three PEO-POSS(5-1) systems in order to determine the effect of POSS alkyl substituent length on ion transport. In **Figure 7a** we see that upon salt addition, the conductivity for all three PEO-POSS(5-1)

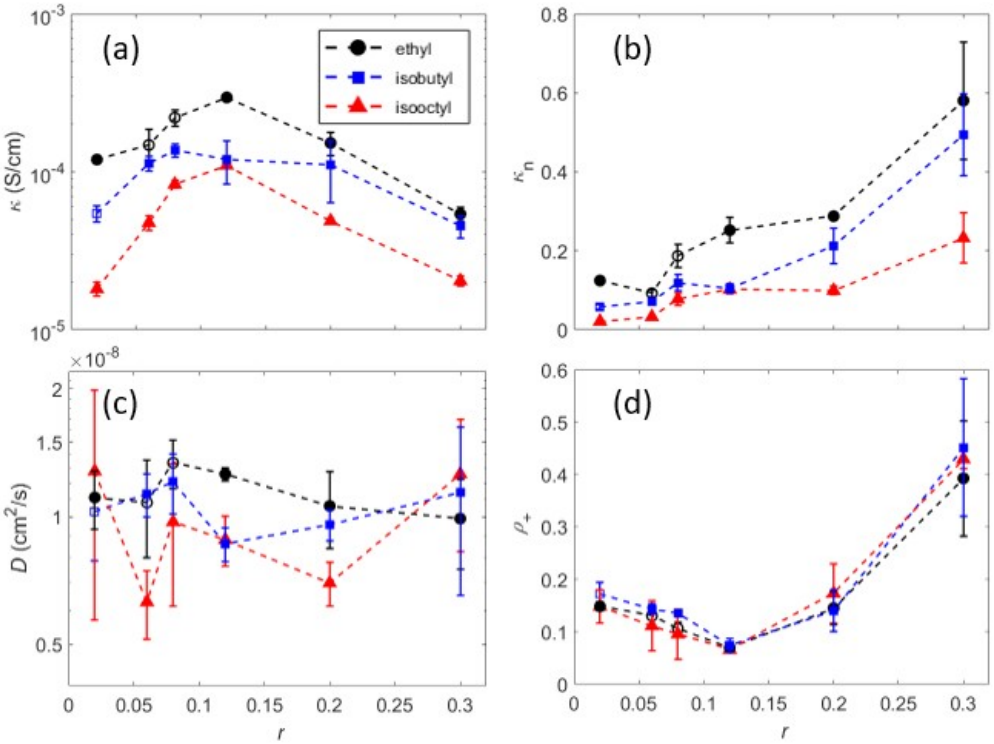

Figure 7. (a) Ionic conductivity from ac impedance spectroscopy of symmetric cells with blocking electrodes. (b) Normalized conductivity, κ_n, using PEO (10 kg mol^{-1}) data. For all salt concentrations, the normalized conductivity decreases as we increase the alkyl substituent length. (c) Salt diffusion coefficient from restricted

diffusion measurements in a lithium symmetric cell. (d) Current fractions calculated from the Bruce-Vincent method using a lithium symmetric cell. Data was taken at 70 °C. The solid markers denote ordered morphologies while open face markers correspond to a disordered phase.

polymers increase until they reach a maximum at around r = 0.12 before decreasing at higher salt concentrations. Ionic conductivity in polymer electrolytes depends on both charge concentration and segmental motion.[24] The glass transition temperature is a simple measure of this segmental relaxation. In our system, the glass transition temperature increases as salt is added (see **Figures S8-S10**) due to ion and polymer associations, from -45 °C at r = 0.08 to -15 °C at r = 0.30 (all of the PEO-POSS(5-1) samples exhibit similar behavior; see **Figure S11**). The peak in the conductivity curves in **Figure 7a** arises due to the interplay between the increase in charge carrier concentration and the slowing down of segmental relaxation.

We can account for the volume fraction of the conducting phase, φ_c, to get a better idea of the differences in intrinsic conductivities across the three systems by utilizing the following equation: $\kappa_n = \kappa_{PEOPOSS}\varphi_c^{-1}\kappa_{PEO}^{-1}$, where κ_{PEO} is the ionic conductivity of PEO (10 kg mol^{-1}) at 70 °C. Previous studies suggest that the ionic conductivity of PEO/LiTFSI mixtures is independent of molecular weight when it exceeds 2 kg mol^{-1}.[52] Increasing the length of the alkyl substituents reduces φ_c at fixed chain length. The plot of normalized conductivity, κ_n, versus POSS silica cage alkyl substituent is shown in **Figure 7b**. Even after accounting for differences in φ_c (see **Figure S14**), the ethyl samples show the highest conductivity, especially in the vicinity of the conductivity maximum. It is perhaps surprising that the greatest normalized conductivity is at the highest salt concentration, r = 0.30. We posit that at high salt concentration, some of the LiTFSI molecules are located in the POSS-rich microphase due to entropic reasons. This will result in a lower salt concentration in the conducting PEO-rich domains, which, in turn, will increase the intrinsic conductivity of these domains as the conductivity of PEO decreases with increasing salt concentration for r > 0.10.[47] The concentration dependence of the salt diffusion coefficient is shown in **Figure 7c**. Neither salt concentration nor alkyl chain length has a strong influence on this parameter, which falls around 10^{-8} cm^2 s^{-1} for all three PEO-POSS(5-1) systems. The concentration dependence of the current fraction shown in **Figure 7d** is similar to that reported for SEO/LiTFSI mixtures and is independent of alkyl chain length.[47]

We compare the mechanical properties of neat PEO-POSS(5-1) to neat PEO(20) with a molecular weight of 20 kg mol^{-1} and neat

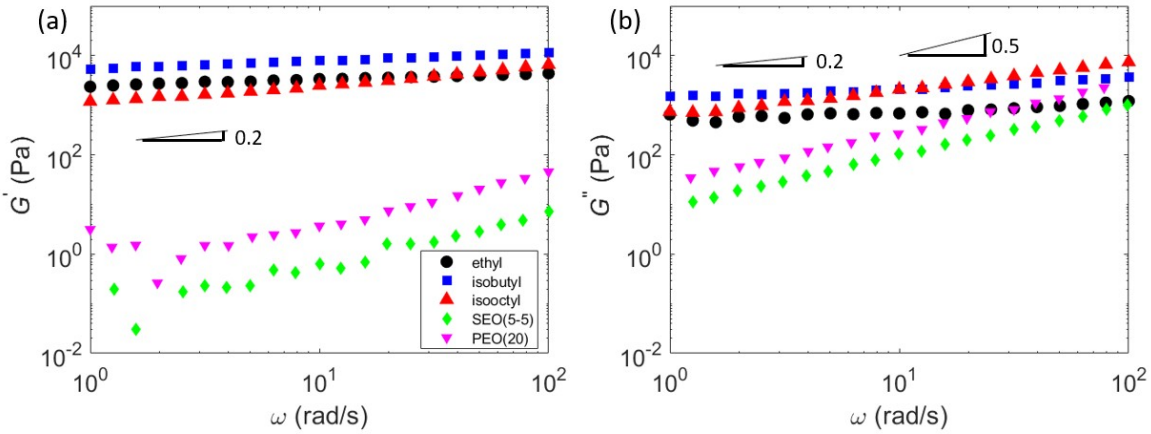

SEO(5-5) which has two blocks of molecular weight 5 kg mol^{-1}. (We choose SEO(5-5) because it exhibits lamellar order.) The storage modulus, G', of the PEO-POSS(5-1) polymers, shown in **Figure 8a**, is a weak function of frequency, typical of solid-like polymers. The magnitude of G' of all three of our PEO-POSS(5-1) polymers is similar. In the low frequency limit, $G' \sim \omega^{0.2}$ for all three PEO-POSS(5-1) polymers. Amongst the polymers covered in this study, the isobutyl sample exhibits the highest storage modulus. G' of PEO-POSS(5-1) polymers is higher than that of PEO(20) and SEO(5-5) by factors between 10^2 and 10^3. The frequency dependence of the loss modulus, G'', is shown in **Figure 8b**. G'' is a weak function of frequency for PEO-POSS(5-1) polymers. In the low frequency limit, $G'' \sim \omega^{0.2}$ for the ethyl and isobutyl samples. For the isooctyl sample $G'' \sim \omega^{0.5}$. At high frequencies, G'' of these polymers

is comparable to that of PEO(20) and SEO(5-5). At low frequencies, G'' of PEO-POSS(5-1) polymers is about a factor of 10 higher than SEO(5-5). Both G' and G'' of PEO(20) and SEO(5-5) decrease rapidly with decreasing frequency.

Figure 8. (a) Storage and (b) loss moduli as a function of frequency for PEO-POSS(5-1), SEO(5-5), and PEO(20). All three PEO-POSS(5-1) polymers exhibit greater mechanical rigidity than SEO(5-5) and PEO(20).–

CONCLUSIONS

We have synthesized and characterized a set of three PEO-POSS(5-1) block copolymer electrolytes with ethyl, isobutyl, and isooctyl substituents on the POSS silica cage. These electrolytes primarily exhibit lamellar morphologies. If only interactions between the salt and PEO were important, then changing the monomer structure of the non-conducting block would have a minimal effect on both thermodynamics and transport. We show, however, that this is not the case. Increasing the length of the POSS alkyl chain substituent leads to a smaller salt concentration window for disorder. In the isooctyl case, no disordered window is observed. Instead, we find coexisting ordered phases that are absent in the ethyl and isobutyl samples. The ethyl samples exhibit the highest ionic conductivity even after normalizing for the volume fraction of conducting phase. The salt diffusion coefficient and current ratio are not affected by the alkyl substituent length. These results indicate that the ethyl systems are optimal for ion transport applications. Further investigation is needed to better understand the relationship between the thermodynamic behavior and ion transport in these hybrid organic-inorganic systems.

ACKNOWLEDGEMENTS

This work was intellectually led by the Joint Center for Energy Storage Research (JCESR), an Energy Innovation Hub funded by the U.S. Department of Energy, Office of Science, Office of Basic Energy Science, under Contract No. **DE-AC02-06CH11357**, which supported both synthesis and characterization work conducted by K.W.G. under the supervision of N.P.B. Work at the Donner Lab, the Molecular Foundry, and the Advanced Light Source, which is a DOE Office of Science User Facility, was supported by Contract No. **DE-AC02-05CH11231**. Work at the Stanford Synchrotron Radiation Light Source, a user facility at SLAC National Accelerator Laboratory, was supported by the U.S. Department of Energy, Office of Science, Office of Basic Energy Science under Contract No. **DE-AC02-76SF00515**. K.W.G. acknowledges funding from a National Defense and Science Engineering Graduate Fellowship.

CONFLICTS OF INTEREST

The authors declare no competing financial interest.

LIST OF SYMBOLS

SEO	polystyrene-b-poly(ethylene oxide)
PEO-POSS	poly(ethylene oxide)-b-polyhedral oligomeric silsesquioxane
PEO	poly(ethylene oxide)
POSS	polyhedral oligomeric silsesquioxane
LiTFSI	lithium bis(trifluoromethanesulfonyl)imide
r	ratio of lithium to ethylene oxide moieties
–R	alkyl substituent group on POSS silica cage
M_{POSS}	molar mass of POSS (g/mol)
M_{PEO}	molar mass of PEO (g/mol)
$f_{EO/LiTFSI}$	volume fraction of EO and LiTFSI phase
N	degree of polymerization
SAXS	small angle x-ray scattering
I	scattering intensity
q	scattering vector (nm^{-1})
I_{abs}	absolute scattering intensity (cm^{-1})
κ	ionic conductivity (S/cm)

ρ_+	current fraction
$R_{i,0}$	initially measured interfacial resistance
$R_{i,0}$	interfacial resistance measured at steady-state
ΔV	applied potential
i_Ω	measure of the initial current, as defined as the ratio of applied potential to sum of bulk and interfacial resistances
$t_{+,ss}$	steady-state cationic transference number
D	salt diffusion coefficient (cm^2/s)
q^*, $2q^*$, $3q^*$	scattering peaks
FWHM	full-width-half-max
TEM	transmission electron microscopy
d	domain spacing
LAM	lamellar
DIS	disordered
COEX/LAM	coexistence of ordered lamellar phases
φ_c	volume fraction of conducting phase
κ_n	normalized conductivity
$\kappa_{PEOPOSS}$	conductivity of PEO-POSS (S/cm)
κ_{PEO}	conductivity of PEO (S/cm)
ω	angular frequency
G'	storage modulus
G''	loss modulus

REFERENCES AND NOTES

(1) Fenton, D. E.; Parker, J. M.; Wright, P. V. Complexes of Alkali Metal Ions with Poly(Ethylene Oxide). *Polymer.* **1973**, *14* (11), 589.

(2) Tarascon, J. M.; Armand, M. Issues and Challenges Facing Rechargeable Lithium Batteries. *Nature* **2001**, *414* (6861), 359–367.

(3) Goodenough, J. B.; Kim, Y. Challenges for Rechargeable Li Batteries. *Chem. Mater.* **2010**, *22* (3), 587–603.

(4) Armand, M. Polymer Solid Electrolytes - an Overview. *Solid State Ionics* **1983**, *9–10,* 745–754.

(5) Balsara, N. P.; Newman, J. Comparing the Energy Content of Batteries, Fuels, and Materials. *J. Chem. Educ.* **2013**, *90* (4), 446–452.

(6) Monroe, C.; Newman, J. The Impact of Elastic Deformation on Deposition Kinetics at Lithium/Polymer Interfaces. *J. Electrochem. Soc.* **2005**, *152* (2), A396.

(7) Singh, M.; Odusanya, O.; Park, M. J.; Iatrou, H.; Wilmes, G. M.; Eitouni, H. B.; Fragouli, P.; Patel, A. J.; Hadjichristidis, N.; Balsara, N. P.; Effect of Molecular Weight on the Mechanical and Electrical Properties of Block Copolymer Electrolytes. *Macromolecules* **2007**, *40* (13), 4578–4585.

(8) Villaluenga, I.; Chen, X. C.; Devaux, D.; Hallinan, D. T.; Balsara, N. P. Nanoparticle-Driven Assembly of Highly Conducting Hybrid Block Copolymer Electrolytes. *Macromolecules* **2015**, *48* (2), 358–364.

(9) Soo, P. P.; Huang, B.; Jang, Y.-I.; Chiang, Y.-M.; Sadoway, D. R.; Mayes, A. M. Rubbery Block Copolymer Electrolytes for Solid-State Rechargeable Lithium Batteries. *J. Electrochem. Soc.* **1999**, *146* (1), 32.

(10) Ruzette, A.-V. G.; Soo, P. P.; Sadoway, D. R.; Mayes, A. M. Melt-Formable Block Copolymer Electrolytes for Lithium Rechargeable Batteries. *J. Electrochem. Soc.* **2002**, *148* (6), A537.

(11) Kosonen, H.; Valkama, S.; Hartikainen, J.; Eerikäinen, H.; Torkkeli, M.; Jokela, K.; Serimaa, R.; Sundholm, F.; Ten Brinke, G.; Ikkala, O. Mesomorphic Structure of Poly(Styrene)-Block-Poly(4-Vinylpyridine) with Oligo(Ethylene Oxide)Sulfonic Acid Side Chains as a Model for Molecularly Reinforced Polymer Electrolyte. *Macromolecules* **2002**, *35* (27), 10149–10154.

(12) Trapa, P. E.; Huang, B.; Won, Y.-Y.; Sadoway, D. R.; Mayes, A. M. Block Copolymer Electrolytes Synthesized by Atom Transfer Radical Polymerization for Solid-State, Thin-Film Lithium Batteries. *Electrochem. Solid-State Lett.* **2002**, *5* (5), A85.

(13) Epps, T. H.; Bailey, T. S.; Waletzko, R.; Bates, F. S. Phase Behavior and Block Sequence Effects in Lithium Perchlorate-Doped Poly(Isoprene-b-Styrene-b-Ethylene Oxide) and Poly(Styrene-b-Isoprene-b-Ethylene Oxide) Triblock Copolymers. *Macromolecules* **2003**, *36* (8), 2873–2881.

(14) Cho, B.-K.; Jain, A.; Gruner, S. M.; Wiesner, U. Mesophase Structure-Mechanical and Ionic Transport Correlations in Extended Amphiphilic Dendrons. **2004**, *305*, 1598–1602.

(15) Panday, A.; Mullin, S.; Gomez, E. D.; Wanakule, N.; Chen, V. L.; Hexemer, A.; Pople, J.; Balsara, N. P. Effect of Molecular Weight and Salt Concentration on Conductivity of Block Copolymer Electrolytes. *Macromolecules* **2009**, *42* (13), 4632–4637.

(16) Young, W. S.; Epps, T. H. Salt Doping in PEO-Containing Block Copolymers: Counterion and Concentration Effects. *Macromolecules* **2009**, *42* (7), 2672–2678.

(17) Mullin, S. A.; Stone, G. M.; Panday, A.; Balsara, N. P. Salt Diffusion Coefficients in Block Copolymer Electrolytes. *J. Electrochem. Soc.* **2011**, *158* (6), A619.

(18) Gunkel, I.; Thurn-Albrecht, T. Thermodynamic and Structural Changes in Ion-Containing Symmetric Diblock Copolymers: A Small-Angle X-Ray Scattering Study. *Macromolecules* **2012**, *45* (1), 283–291.

(19) Young, W. S.; Epps, T. H. Ionic Conductivities of Block Copolymer Electrolytes with Various Conducting Pathways: Sample Preparation and Processing Considerations. *Macromolecules* **2012**, *45* (11), 4689–4697.

(20) Teran, A. A.; Balsara, N. P. Thermodynamics of Block Copolymers with and without Salt. *J. Phys. Chem. B* **2014**, *118* (1), 4–17.

(21) Irwin, M. T.; Hickey, R. J.; Xie, S.; So, S.; Bates, F. S.; Lodge, T. P. Structure-Conductivity Relationships in Ordered and Disordered Salt-Doped Diblock Copolymer/Homopolymer Blends. *Macromolecules* **2016**, *49* (18), 6928–6939.

(22) Loo, W. S.; Jiang, X.; Maslyn, J. A.; Oh, H. J.; Zhu, C.; Downing, K. H.; Balsara, N. P. Reentrant Phase Behavior and Coexistence in Asymmetric Block Copolymer Electrolytes. *Soft Matter* **2018**, *14* (15), 2789–2795.

(23) Sethi, G. K.; Jiang, X.; Chakraborty, R.; Loo, W. S.; Villaluenga, I.; Balsara, N. P. Anomalous Self-Assembly and Ion Transport in Nanostructured Organic-Inorganic Solid Electrolytes. *ACS Macro Lett.* **2018**, *7* (9), 1056–1061.

(24) Ratner, M. A.; Johansson, P.; Shriver, D. F. Polymer Electrolytes: Ionic Transport Mechanisms and Relaxation Coupling. *MRS Bull*. **2000**, *25*, 31.

(25) Li, G.; Charles, U. P. Polyhedral Oligomeric Silsesquioxane (POSS) Polymers, Copolymers, and Resin Nanocomposites. *Macromol. Contain. Met. Met. Elem. Gr. IVA Polym.* **2005**, *4* (3), 79–131.

(26) Matějka, L.; Strachota, A.; Pleštil, J.; Whelan, P.; Steinhart, M.; Šlouf, M. Epoxy Networks Reinforced with Polyhedral Oligomeric Silsesquioxanes (POSS). Structure and Morphology. *Macromolecules* **2004**, *37* (25), 9449–9456.

(27) Ni, Y.; Zheng, S.; Nie, K. Morphology and Thermal Properties of Inorganic-Organic Hybrids Involving Epoxy Resin and Polyhedral Oligomeric Silsesquioxanes. *Polymer (Guildf).* **2004**, *45* (16), 5557–5568.

838(28) Fina, A.; Tabuani, D.; Frache, A.; Camino, G. Polypropylene-Polyhedral
839 Oligomeric Silsesquioxanes (POSS) Nanocomposites. *Polymer.* **2005**,
840 *46*, 7855–7866.
841(29) Pracella, M.; Chionna, D.; Fina, A.; Tabuani, D.; Frache, A.; Camino, G.
842 Polypropylene-POSS Nanocomposites: Morphology and Crystallization
843 Behaviour. *Macromol. Symp.* **2006**, *234*, 59–67.
844(30) Perrin, F. X.; Panaitescu, D. M.; Frone, A. N.; Radovici, C.; Nicolae, C.
845 The Influence of Alkyl Substituents of POSS in Polyethylene
846 Nanocomposites. *Polymer.* **2013**, *54* (9), 2347–2354.
847(31) Heeley, E. L.; Hughes, D. J.; El Aziz, Y.; Williamson, I.; Taylor, P. G.;
848 Bassindale, A. R. Properties and Self-Assembled Packing Morphology of
849 Long Alkyl-Chained Substituted Polyhedral Oligomeric Silsesquioxanes
850 (POSS) Cages. *Phys. Chem. Chem. Phys.* **2013**, *15* (15), 5518–5529.
851(32) Lu, Y. S.; Kuo, S. W. Functional Groups on POSS Nanoparticles Influence
852 the Self-Assembled Structures of Diblock Copolymer Composites. *RSC*
853 *Adv.* **2014**, *4* (66), 34849–34859.
854(33) Heeley, E. L.; Hughes, D. J.; El Aziz, Y.; Taylor, P. G.; Bassindale, A. R.
855 Morphology and Crystallization Kinetics of Polyethylene/Long Alkyl-
856 Chain Substituted Polyhedral Oligomeric Silsesquioxanes (POSS)
857 Nanocomposite Blends: A SAXS/WAXS Study. *Eur. Polym. J.* **2014**, *51*
858 (1), 45–56.
859(34) Niemczyk, A.; Dziubek, K.; Sacher-Majewska, B.; Czaja, K.; Dutkiewicz,
860 M.; Marciniec, B. Study of Thermal Properties of Polyethylene and

Polypropylene Nanocomposites with Long Alkyl Chain-Substituted POSS Fillers. *J. Therm. Anal. Calorim.* **2016**, *125* (3), 1287–1299.

(35) Ueda, K.; Tanaka, K.; Chujo, Y. Synthesis of POSS Derivatives Having Dual Types of Alkyl Substituents and Their Application as a Molecular Filler for Low-Refractive and Highly Durable Materials. *Bull. Chem. Soc. Jpn.* **2017**, *90* (2), 205–209.

(36) Miao, J.; Cui, L.; Lau, H. P.; Mather, P. T.; Zhu, L. Self-Assembly and Chain-Folding in Hybrid Coil-Coil-Cube Triblock Oligomers of Polyethylene-b-Poly(Ethylene Oxide)-b-Polyhedral Oligomeric Silsesquioxane. *Macromolecules* **2007**, *40* (15), 5460–5470.

(37) Yu, X.; Zhong, S.; Li, X; Tu, Y.; Yang, S.; Van Horn, R.; Ni, C.; Pochan, D. J.; Quirk, R. P.; Wesdemiotis, C.; Zhang, W.; Cheng, S. Z. D. A Giant Surfactant of Polystyrene– (Carboxylic Acid-Functionalized Polyhedral Oligomeric Silsesquioxane) Amphiphile with Highly Stretched Polystyrene Tails in Micellar Assemblies. *J. Am. Chem. Soc.* **2010**, *132* (47), 16741-16744.

(38) Huang, M.; Hsu, C.; Wang, J.; Mei, S.; Dong, X.; Li, Y.; Li, M.; Liu, H.; Zhang, W.; Aida, T.; Zhang, W.; Yue, K.; Cheng, S. Z. D. Selective Assemblies of Giant Tetrahedra via Precisely Controlled Positional Interactions. *Science.* **2015**, *348* (6233), 424–428.

(39) Sax, J.; Ottino, J. M. Modeling of transport of small molecules in polymer blends:

Application of effective medium theory. *Polymer Engineering and Science.* **1983**, *23* (3), 165–176.

(40) Kambe, Y.; Arge, C. G.; Patel, S. N.; Stoykovich, M. P.; Nealey, P. F. Ion Conduction in Microphase-Separated Block Copolymer Electrolytes. *Electrochem. Soc. Interface* **2017,** *26,* 61–67.

(41) Hexemer, A.; Bras, W.; Glossinger, J.; Schaible, E.; Gann, E.; Kirian, R.; MacDowell, A.; Church, M.; Rude, B.; Padmore, H. A SAXS/WAXS/GISAXS Beamline with Multilayer Monochromator. *J. Phys. Conf. Ser.* **2010**, *247*.

(42) Ilavsky, J. Nika: Software for Two-Dimensional Data Reduction. *J. Appl. Crystallogr.* **2012**, *45* (2), 324–328.

(43) Newman, J.; Chapman, T. W. Restricted Diffusion in Binary Solutions. *AIChE J.* **1973**, *19* (2), 343–348.

(44) Bruce, P. G.; Hardgrave, M. T.; Vincent, C. A. Steady State Current Flow in Solid Binary Electrolyte Cells. *J. Electroanal. Chem. Interfacial Electrochem.* **2002**, *271* (1–2), 27–34.

(45) Galluzzo, M. D.; Maslyn, J. A.; Shah, D. B.; Balsara, N. P. Ohm’s law for ion conduction in lithium and beyond-lithium battery electrolytes. *The Journal of Chemical Physics.* **2019**, *151.*

(46) Balsara, N. P.; Newman, J. Relationship between Steady-State Current in Symmetric Cells and Transference Number of Electrolytes

Comprising Univalent and Multivalent Ions. *J. Electrochem. Soc.* **2015**, *162* (14), A2720 – A2722.

(47) Villaluenga, I.; Pesko, D. M.; Timachova, K.; Feng, Z.; Newman, J.; Srinivasan, V.; Balsara, N. P. Negative Stefan-Maxwell Diffusion Coefficients and Complete Electrochemical Transport Characterization of Homopolymer and Block Copolymer Electrolytes. *J. Electrochem. Soc.* **2015**, *162* (3), A398–A405.

(48) Schauser, N. S.; Harry, K. J.; Parkinson, D. Y.; Watanabe, H.; Balsara, N. P. Lithium Dendrite Growth in Glassy and Rubbery Nanostructured Block Copolymer Electrolytes. *J. Electrochem. Soc.* **2018**, *165* (11), A2766–A2773

(49) Leibler, L. Theory of Microphase Separation in Block Copolymers. *Macromolecules* **1980**, *13* (6), 1602–1617.

(50) Thelen, J. L.; Teran, A. A.; Wang, X.; Garetz, B. A.; Nakamura, I.; Wang, Z. G.; Balsara, N. P. Phase Behavior of a Block Copolymer/Salt Mixture through the Order-to-Disorder Transition. *Macromolecules* **2014**, *47* (8), 2666–2673.

(51) Shim, J.; Bates, F. S.; Lodge, T. P. Superlattice by charged block copolymer self-assembly. *Nature Communications.* **2019**, *10,* 2108.

(52) Teran, A. A.; Tang, M. H.; Mullin, S. A.; Balsara, N. P. Effect of molecular weight on conductivity of polymer electrolytes. *Solid State Ionics.* **2011**, *203,* 18–21.

GRAPHICAL ABSTRACT

Kevin W. Gao, Xi Jiang, Zach J. Hoffman, Gurmukh K. Sethi, Saheli Chakraborty, Irune Villaluenga, Nitash P. Balsara

Optimizing the Monomer Structure of Polyhedral Oligomeric Silsesquioxane (POSS) for Ion Transport in Hybrid Organic-Inorganic Block Copolymers

Poly(ethylene oxide)-*b*-polyhedral oligomeric silsesquioxane (PEO-POSS) mixed with lithium salt is a nanostructured hybrid organic-inorganic block copolymer electrolyte that may enable lithium metal batteries. Three PEO-POSS electrolytes which only differ by their POSS substituents (ethyl, isobutyl, isooctyl) are synthesized and characterized. Salt-induced mixing of the two blocks becomes less effective as the length of the POSS alkyl chain substituent is increased. The ethyl substituent is shown to be optimal for ion

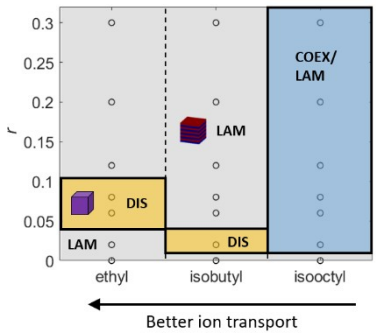

transport.